The Impact of Land Cover Types on the Urban Heat Island Effect: A Case Study of Xi'an

Wangqiang Xu[1, *]

[1]School of Geomatics and Urban Spatial Informatics, Beijing University of Civil Engineering and Architecture, Beijing, China

*Corresponding Author: 2108160322005@stu.bucea.edu.cn

Abstract

The urban heat island effect is a typical urban climate phenomenon, and its formation and intensity are closely related to land cover types. This study uses Landsat data from Xi'an in 2016 to invert land surface temperature (LST) based on the radiation transfer equation method. Through statistical analysis, ArcGIS buffer zone analysis, and other methods, the study investigates the impact of land cover types on the urban heat island effect in Xi'an. The conclusions are as follows: it is found that unused land and built-up areas promote the urban heat island effect, while vegetation and water bodies help alleviate it.

Keywords

Urban heat island effect; Land surface temperature; Statistical analysis; ArcGIS buffer analysis; Xi'an.

1. INTRODUCTION

It is well known that the intensity of the urban heat island effect is closely related to city size, urban surface features, anthropogenic heat release, topography, and meteorological conditions[1-5]. With continuous urbanization, humans have greatly changed the original natural landscape. The original open space is now full of tall buildings, man-made building materials have replaced the natural terrain, and many environmental problems caused by urbanization have become more and more serious. One of the most important impacts on the climate is the urban heat island effect and the emission of greenhouse gases[6-12].

The urban heat island effect will not only affect the local or regional climate of the city, but also affect the circulation of land, ocean and river flow, and negatively affect the living comfort of urban residents, the spread of air pollution and energy consumption.

For example, Ruey-Lung Hwang et al.[13]quantified the impact of UHI on air conditioning energy consumption and overheating risk in buildings. They applied EnergyPlus simulations to analyze 1496 micro-scale areas in Tainan, and the results showed that residential areas in urban and suburban areas are at risk of overheating within 3 to 5 months. And that from May to October, the natural ventilation potential of residential areas in rural and surrounding areas is greater than that in urban areas. The energy consumption of air conditioners in rural areas is less than that in cities and suburbs.

The development of thermal remote sensing provides a good solution to the flaw observed in conventional monitoring of urban heat islands[14]. Such techniques can quantitatively and effectively monitor the distribution characteristics of urban heat islands as well as the periodic and dynamic changes in urban thermal environments[15].

ISSN: 2472-3703 DOI: 10.6911/WSRJ.202503_11(3).0005

The traditional heat island effect uses weather station data to select several temperature indicators to analyze changes in the characteristics of a regional heat island[16-18]. To obtain large-area continuous land surface temperature information, the spatial resolution is low [19]. The remote sensing monitoring method can solve this problem very well, that is, to conduct large-scale synchronous observation of the earth at a small cost, with high spatial resolution, easy to find the macroscopic laws of spatial distribution, fast monitoring speed, and convenient update[20].

Felipe Ferreira Monteiro et al.[21]analysed the urban heat island effect in 21 metropolitan areas in Brazil during the dry season in the past 17 years using the surface temperature, NDVI, and average reflectance produced by MODIS sensors. The results showed that urban heat islands existed in all metropolitan areas. different periods of the day.

Based on the above background, this study extracted rich land cover information based on Landsat remote sensing images of Xi'an City, and further analysed the impact of urban land cover on surface temperature and heat budget components. This study aims to understand the impact of land cover pattern on urban surface thermal environment in Xi'an, and provide basic research support for optimizing urban landscape and mitigating urban heat island effect. Due to rapid urbanization and landscape transformation, the land cover pattern of Xi'an has undergone substantial changes, which has resulted in a series of urban thermal environmental problems.

2. MATERIALS AND METHODS

2.1. Study Region and Data

Xi'an is located in the northwest of China, in the central part of the Guanzhong Plain, bordering the Weihe River in the north and the Qinling Mountains in the south, between 107°40′-109°49′east longitude and 33°42′-34°45′ north latitude. As of the end of 2022, the city has 11 districts and 2 counties under its jurisdiction(Figure 1).

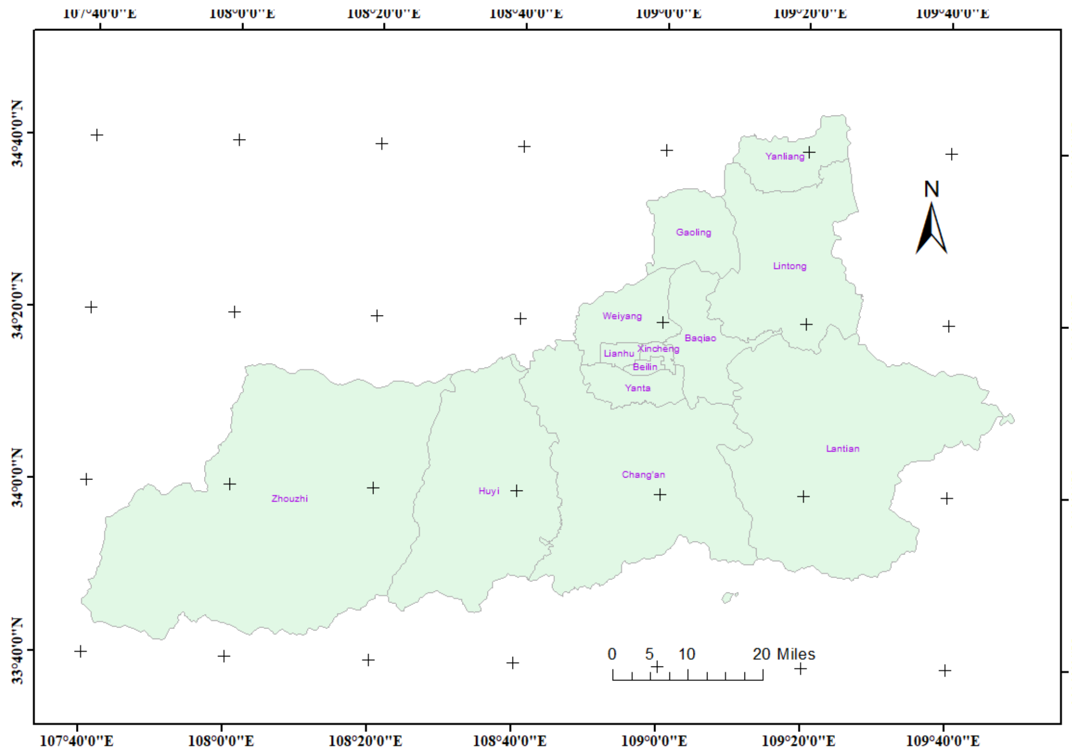

Figure 1. Xi'an Administrative Division Map

ISSN: 2472-3703 DOI: 10.6911/WSRJ.202503_11(3).0005

This paper takes the Landsat data of Xi'an on June 17, 2016 as the research object, and inverts the surface temperature of the reflection image after remote sensing preprocessing based on the radiation transfer equation method. At the same time, through supervised classification, the land cover type map of Xi'an in 2016 is obtained.

2.2. Methods

2.2.1 Land Surface temperature retrieval method

In this paper, the radiative transfer equation method[22] is used to invert the land surface temperature on the processed Landsat data. In the ground-atmosphere radiation transmission of thermal infrared remote sensing, both the ground and the atmosphere are sources of thermal infrared radiation, and the radiant energy passes through the atmosphere many times and is absorbed, scattered and emitted by the atmosphere. Therefore, the total radiance received by the remote sensor is divided into three parts, that is, surface emission energy, atmospheric upward radiation, and atmospheric downward radiation[23], that is, the radiation transfer equation is:

$$L_{\lambda} = [\varepsilon B(T_S) + (1-\varepsilon)L\downarrow]\tau + L\uparrow \tag{1}$$

Among them, $L\downarrow$ and $L\uparrow$ are atmospheric upward radiation and atmospheric downward radiation with a wavelength of λ, respectively, and L_{λ} is the thermal infrared radiation brightness received by the remote sensor with a wavelength of λ. The units of $L\downarrow$, $L\uparrow$, and L_{λ} are all w/(m2 •μm•sr), ε is the specific emissivity of the surface, τ is the atmospheric transmittance from the ground to the remote sensor, and $B(T_S)$ is the Planckian blackbody radiance at the true surface temperature TS. Then, according to the radiation transfer equation, the calculation formula of the Planckian blackbody radiance $B(T_S)$ at the true surface temperature T_S is derived:

$$B(T_S) = [L_{\lambda} - L\uparrow - \tau(1-\varepsilon)L\downarrow]/\tau\varepsilon \tag{2}$$

Among them, $L\downarrow$, $L\uparrow$, and τ can be found through the NASA website (https://atmcorr.gsfc.nasa.gov/), and L_{λ} is the value after calibration of thermal infrared band radiation, only the surface specific emissivity ε unknown.

According to Planck's inverse function, T_S can be obtained

$$T_S = K_2 / \ln\left[\frac{K_1}{B(T_S)} + 1\right] \tag{3}$$

For Landsat-5 TM6 image, K1=607.76 w/(m2•μm•sr), K2=1260.56K;

For Landsat-7 ETM+6 image, K1=666.09 W/(m2•μm•sr), K2=1282.71K;

For the Landsat-8 TIRS Band10 image, K1= 774.89 W/(m2•μm•sr), K2= 1321.08K. These can be found in the image header file.

2.2.2 Calculation of surface emissivity(ε)

Do *not* number your paper: This paper uses the Landsat series data from 2016 and the radiation transfer equation to invert the surface temperature. First, the remote sensing image is preprocessed, then the required parameters are obtained using the ENVI band calculation tool, and finally the surface temperature is obtained using formulas (2) and (3). For the key unknown parameters in the thermal infrared band, the surface specific emissivity needs to be estimated.

ISSN: 2472-3703 DOI: 10.6911/WSRJ.202503_11(3).0005

According to the theory of Qin Zhihao et al.[24], the surface can be roughly divided into three types of structures: water bodies, natural surfaces, and towns. It is generally believed that the specific emissivity of water bodies is similar to that of black bodies, and is estimated by ε water = 0.995; the formula for calculating the specific emissivity of natural surfaces and urban surfaces is as follows:

$$\varepsilon_{\text{natural}} = 0.9625 + 0.0614P_v - 0.0461P_v \times P_v \tag{4}$$

$$\varepsilon_{\text{town}} = 0.9589 + 0.086P_v - 0.067P_v \times P_v \tag{5}$$

In the formula, ε_{water} is the specific emissivity of the surface of the water body, $\varepsilon_{\text{natural}}$ surface is the surface specific emissivity of the natural surface, $\varepsilon_{\text{town}}$ is the surface specific emissivity of the town; PV is the vegetation coverage, and its calculation formula is as follows[25]:

$$P_v = \frac{NDVI - NDVI_S}{NDVI_V - NDVI_S} \tag{6}$$

$NDVI_S$ and $NDVI_V$ are the NDVI values of vegetation and bare soil respectively. Generally, when the NDVI of a pixel exceeds 0.7, then this pixel is considered to be complete vegetation, and P_V=1 is taken at this time; when the NDVI value of a pixel is less than 0.05, The pixel can be completely regarded as bare soil[26], and PV=0 is taken at this time; therefore, $NDVI_S$=0.05 and $NDVI_V$=0.7 can be used for approximate estimation.

When NDVI⩽0, the surface is regarded as a water body;

When 0<NDVI<0.7, the surface is regarded as a town;

When NDVI ⩾ 0.7, the ground surface is regarded as a natural surface

2.2.3 Verification of the inversion results of land surface temperature

Due to the lack of real-time surface temperature data in Xi'an, it is impossible to accurately verify the inversion results of surface temperature. This paper uses the 0cm ground temperature data under the China Meteorological Data Network and the China Ground International Exchange Station Climate Data Daily Value Dataset (V3.0) to compare and verify the surface temperature inversion results from 2010 to 2019; after comparison with meteorological data, the temperature inversion results have a certain reference value. The comparison is shown in Table 1.

Table 1. The Results of Land Surface Temperature Inversion Are Verified

date	Station	Lat/Lon	Mean [°C]	Max [°C]	Min [°C]	Remote sensing image inversion results [°C]
2016-06-17	Jinghe	34°26′N 108°58′E	35.6	61.6	17.9	45.1

ISSN: 2472-3703 DOI: 10.6911/WSRJ.202503_11(3).0005

3. RESULTS ANALYSIS AND DISCUSSION

3.1. Results

The surface temperature was inverted based on the radiation transfer equation method as shown in Figure 2. At the same time, through supervised classification, the land cover type of Xi'an in 2016 was obtained as shown in Figure 3.

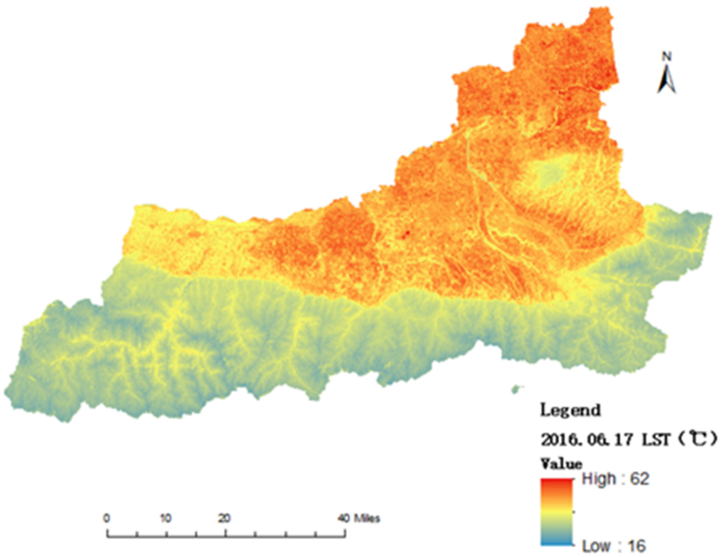

Figure 2. Land Surface temperature distribution map of Xi'an on June 17, 2016

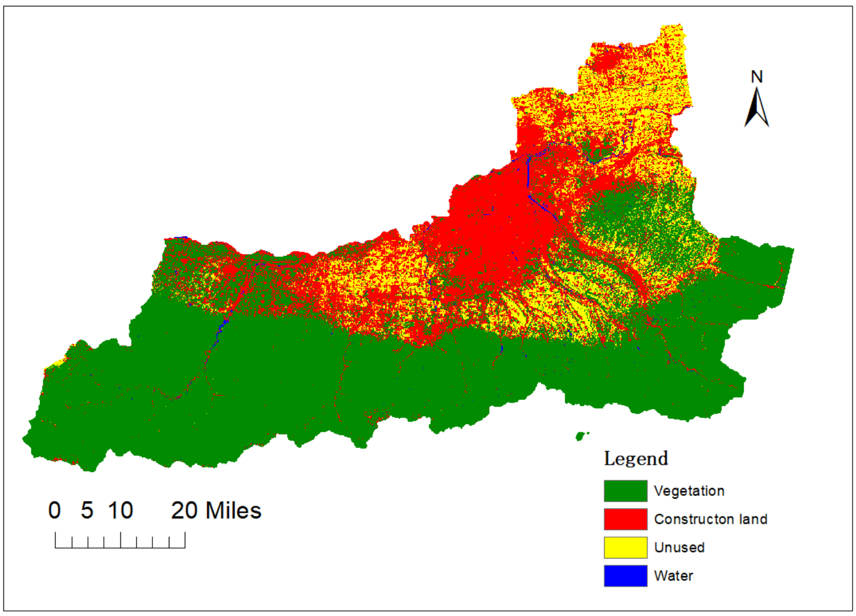

Figure 3. Land Cover Type Map of Xi'an on June 17, 2016

3.2. Statistical analysis of land surface temperature for different land cover

According to the results of land use classification in 2016, convert each land type from a raster file to a vector shapefile in ENVI, open the vector file of each land type with ArcGIS software, and extract the temperature distribution map in 2016 as a mask. Extract the temperature distribution map under different ground objects, and count the temperature average and standard deviation, and draw the temperature statistics table of different land types as shown in Table 2.

ISSN: 2472-3703 DOI: 10.6911/WSRJ.202503_11(3).0005

Table 2. Statistics of Land Surface Temperature for Each Land Type in 2016

Land cover type	Mean [°C]	standard deviation [°C]
vegetation	27.79	5.22
Construction land	40.54	3.54
Water	31.02	3.92
Unused	44.35	3.30

(1) It can be seen from Table 6 that the order of land use types in Xi'an in 2010 from high to low is: unused land > construction land > water body > vegetation. contribution, among which unused land has the greatest impact, and construction land is second only to unused land.

(2) Vegetation and water bodies are conducive to alleviating urban heat island, and the standard deviation of vegetation is larger than that of other land types, because the woodland, grassland, and cultivated land are all divided into a whole, and the vegetation coverage of forest land, grassland, and cultivated land is Varies and naturally affects temperature in different ways.

3.3. Spatial analysis of the relationship between land use types and temperature

In order to further analyse the impact of land cover type on the heat island effect, 8 concentric circular buffer zones within the range of 15-135km were generated from the centre of Xi'an administrative division at a distance of 15km, and the surface area of each buffer zone was extracted. Temperature distribution map, land cover type map, statistics of the mean and standard deviation of surface temperature in each buffer zone, and the area ratio of each land cover type. The statistical data obtained are plotted in Excel as a broken-line statistical chart of the average value of surface temperature, standard deviation, and area proportion of land cover types as a function of the distance from the buffer zone. Among them, the schematic diagram of the buffer zone (Figure 4), the change of the area proportion of land cover type with the distance from the buffer zone (Figure 5), and the change of the mean and standard deviation of the surface temperature with the distance from the buffer zone (Figure 6, Figure 7) are shown in the figure.

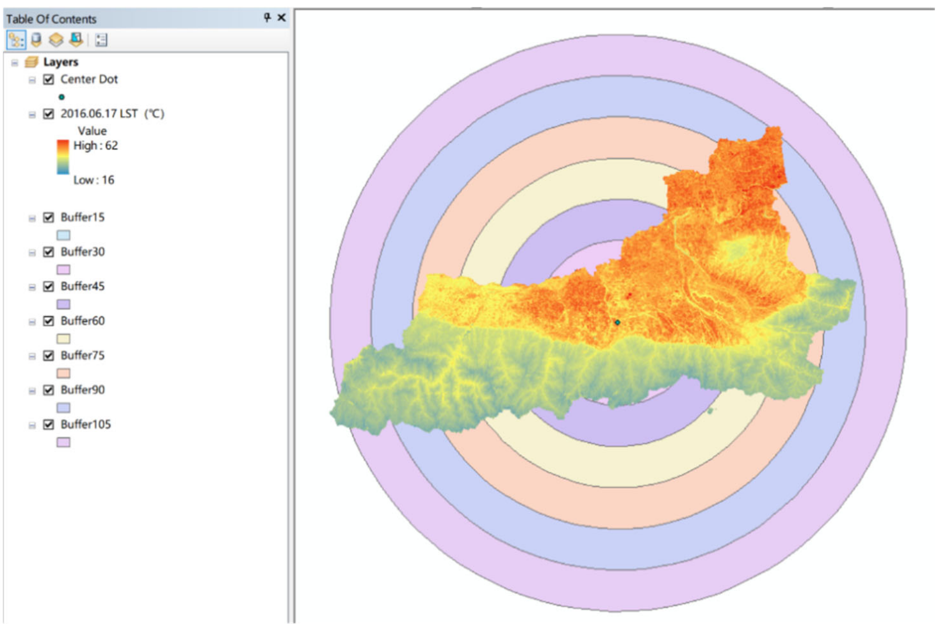

Figure 4. Buffer Diagram

ISSN: 2472-3703 DOI: 10.6911/WSRJ.202503_11(3).0005

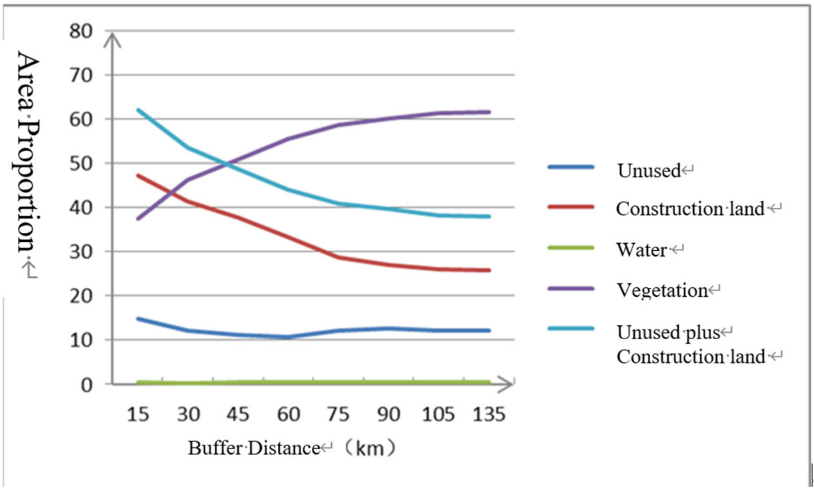

Figure 5. Changes in the Proportion of Land cover type with Distance

It can be seen from Figure 5 that the area proportion of construction land decreases monotonically with the increase of the distance from the buffer zone. It decelerates faster before 75km and slower after 75km; Fast and then slow; unused land is in the decline stage from 15~60km, 60~75km is in the process of increasing and returning to the original area proportion, 75~135km remains basically unchanged, and the water body area proportion is generally low, and basically remains the same with the distance. Change.

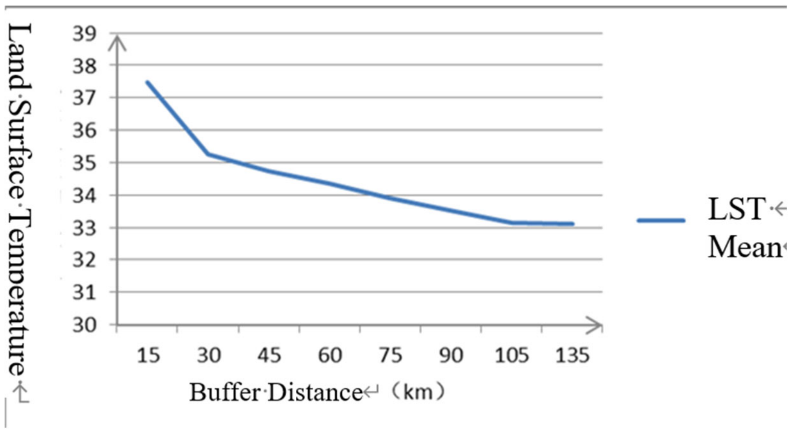

Figure 6. Line graph of Mean of LST changing with distance

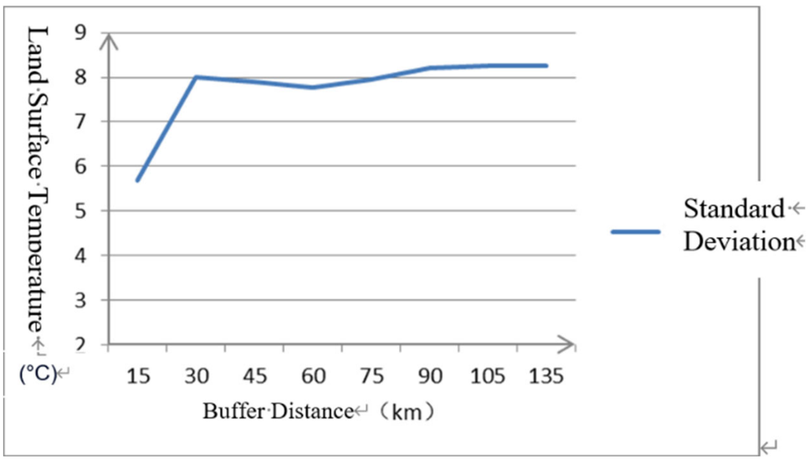

Figure 7. Line graph of surface temperature standard deviation with distance

ISSN: 2472-3703 DOI: 10.6911/WSRJ.202503_11(3).0005

From Figure 6, it can be seen that the average surface temperature changes with distance, which can be roughly divided into three stages: the average surface temperature decreases rapidly at 15-30km, decreases at a slower rate at 30-105km, and basically decreases from 105-135km. constant.

Comparing Figure 5 and Figure 6, it can be found that the change curve of the average land surface temperature with distance is more consistent with the change curve of the proportion of buildings, and most consistent with the change curve of the proportion of unused land + construction land area, indicating that the spatial layout of urban construction is in the to a considerable extent, it determines the structure distribution of the land surface temperature.

It can be seen that the average surface temperature slows down faster than the proportion of unused land + construction land in the range of 15-30 km. This is because the curve of the proportion of unused land + construction land with distance does not take into account the effect of vegetation. It can be seen that vegetation has a mitigation effect on urban heat island;

From Figure 7, it can be seen that the standard deviation of the surface temperature increases rapidly from 15 to 30 km with the increase of the buffer distance, and does not change much after 30 km. The appearance of such an image is due to the fact that within 30 km, the effect of surface objects on the heat island is relatively consistent, mainly for construction land and unused land, and the temperature is relatively concentrated, so the standard deviation of surface temperature is small.

4. CONCLUSIONS

Based on the Landsat data of Xi'an in 2016, this study used the radiation transfer equation method to invert the surface temperature. Through statistical analysis and ArcGIS buffer analysis, it was shown that unused land and construction land have a promoting effect on the urban heat island, while vegetation and water bodies are conducive to alleviating the urban heat island effect. The spatial layout of urban construction determines the structural distribution of surface temperature to a considerable extent.

This study only conducted one year of supervised classification, and did not produce a full-year land cover type map and study its changes. Secondly, the spatial resolution of the Landsat series data is limited, and the multi-spectral is only 30 meters. It is not easy to classify cultivated land, grassland, and forest land, and the classification is not fine enough; at the same time, the temporal resolution of Landsat data is low, and coupled with cloud data coverage, the data quality has declined. In the future, higher-resolution images can be selected to make up for the shortcomings of classification.

5. CONFLICTS OF INTEREST

The authors declare that they have no conflict of interest.

ACKNOWLEDGEMENTS

I am very grateful for the free Landsat satellite remote sensing data provided by USGS.

REFERENCES

[1] R. M. Society, Quarterly Journal of the Royal Meteorological Society. Royal Meteorological Society., 1875.

[2] R. Castriota and J. Tonucci, "Extended urbanization in and from Brazil," Environment and Planning D-Society & Space, vol. 36, no. 3, pp. 512-528, Jun 2018, doi: 10.1177/0263775818775426.

[3] C. L. Gu, "Urbanization: Processes and driving forces," Science China-Earth Sciences, vol. 62, no. 9, pp. 1351-1360, Sep 2019, doi: 10.1007/s11430-018-9359-y.

[4] Y. J. Miao, X. L. Zuo, and H. Y. Fan, "Environmental Study on Harmonious Development of Rural Urbanization Construction under the Horizon," Ekoloji, vol. 28, no. 107, pp. 4615-4623, 2019, Art no. UNSP e107518. [Online]. Available: <Go to ISI>://WOS:000461678300517.

[5] X. R. Zhang et al., "Analysis on Decoupling between Urbanization Level and Urbanization Quality in China," Sustainability, vol. 12, no. 17, Sep 2020, Art no. 6835, doi: 10.3390/su12176835.

[6] Q. F. Huang and Y. Q. Lu, "Urban heat island research from 1991 to 2015: a bibliometric analysis," THEORETICAL AND APPLIED CLIMATOLOGY, vol. 131, no. 3-4, pp. 1055-1067, FEB 2018, doi: 10.1007/s00704-016-2025-1.

[7] L. Ji and W. Zhang, "Fiscal Incentives and Sustainable Urbanization: Evidence from China," Sustainability, vol. 12, no. 1, Jan 2020, Art no. 103, doi: 10.3390/su12010103.

[8] T. G. Lv et al., "Coupling Coordinated Development and Exploring Its Influencing Factors in Nanchang, China: From the Perspectives of Land Urbanization and Population Urbanization," Land, vol. 8, no. 12, Dec 2019, Art no. 178, doi: 10.3390/land8120178.

[9] J. Shang, P. F. Li, L. Li, and Y. Chen, "The relationship between population growth and capital allocation in urbanization," Technological Forecasting and Social Change, vol. 135, pp. 249-256, Oct 2018, doi: 10.1016/j.techfore.2018.04.013.

[10] Y. J. Shi et al., "Independent or Influential? Spatial-Temporal Features of Coordination Level between Urbanization Quality and Urbanization Scale in China and Its Driving Mechanism," International Journal of Environmental Research and Public Health, vol. 17, no. 5, Mar 2020, Art no. 1587, doi: 10.3390/ijerph17051587.

[11] J. S. Wu, D. J. Cheng, Y. Y. Xu, Q. Huang, and Z. Feng, "Spatial-temporal change of ecosystem health across China: Urbanization impact perspective," Journal of Cleaner Production, vol. 326, Dec 2021, Art no. 129393, doi: 10.1016/j.jclepro.2021.129393.

[12] A. L. Zhou, "Research on the Development Path of Agricultural Insurance in the Process of New Urbanization," Agro Food Industry Hi-Tech, vol. 28, no. 3, pp. 1953-1957, May-Jun 2017. [Online]. Available: <Go to ISI>://WOS:000405993200034.

[13] R.-L. Hwang, T.-P. Lin, and F.-Y. Lin, "Evaluation and mapping of building overheating risk and air conditioning use due to the urban heat island effect," Journal of Building Engineering, vol. 32, p. 101726, 2020/11/01/ 2020, doi: https://doi.org/10.1016/j.jobe.2020.101726.

[14] Y. Liu, Q. Li, L. Yang, K. K. Mu, M. Y. Zhang, and J. P. Liu, "Urban heat island effects of various urban morphologies under regional climate conditions," Science of the Total Environment, vol. 743, Nov 2020, Art no. 140589, doi: 10.1016/j.scitotenv.2020.140589.

[15] M. Milelli, F. Bassani, V. Garbero, D. Poggi, J. von Hardenberg, and L. Ridolfi, "Characterization of the Urban Heat and Dry Island effects in the Turin metropolitan area," Urban Climate, vol. 47, Jan 2023, Art no. 101397, doi: 10.1016/j.uclim.2022.101397.

[16] L. L. Zhang, Q. Y. Meng, Z. H. Sun, and Y. X. Sun, "Spatial and Temporal Analysis of the Mitigating Effects of Industrial Relocation on the Surface Urban Heat Island over China," Isprs International Journal of Geo-Information, vol. 6, no. 4, Apr 2017, Art no. 121, doi: 10.3390/ijgi6040121.

[17] Y. H. Liu, X. Y. Fang, Y. M. Xu, S. Zhang, and Q. Z. Luan, "Assessment of surface urban heat island across China's three main urban agglomerations," Theoretical and Applied Climatology, vol. 133, no. 1-2, pp. 473-488, Jul 2018, doi: 10.1007/s00704-017-2197-3.

[18] V. Miles and I. Esau, "Seasonal and Spatial Characteristics of Urban Heat Islands (UHIs) in Northern West Siberian Cities," Remote Sensing, vol. 9, no. 10, Oct 2017, Art no. 989, doi: 10.3390/rs9100989.

[19] W. M. Wang, K. Liu, R. Tang, and S. D. Wang, "Remote sensing image-based analysis of the urban heat island effect in Shenzhen, China," Physics and Chemistry of the Earth, vol. 110, pp. 168-175, Apr 2019, doi: 10.1016/j.pce.2019.01.002.

[20] Y. Abbassi, H. Ahmadikia, and E. Baniasadi, "Impact of wind speed on urban heat and pollution islands," Urban Climate, vol. 44, Jul 2022, Art no. 101200, doi: 10.1016/j.uclim.2022.101200.

[21] F. F. Monteiro, W. A. Gonçalves, L. d. M. B. Andrade, L. M. M. Villavicencio, and C. M. dos Santos Silva, "Assessment of Urban Heat Islands in Brazil based on MODIS remote sensing data," Urban Climate, vol. 35, p. 100726, 2021.

[22] A. D. Klose, "The forward and inverse problem in tissue optics based on the radiative transfer equation: A brief review," Journal of Quantitative Spectroscopy and Radiative Transfer, vol. 111, no. 11, pp. 1852-1853, 2010/07/01/ 2010, doi: https://doi.org/10.1016/j.jqsrt.2010.01.020.

[23] Q. Weng, "Thermal infrared remote sensing for urban climate and environmental studies: Methods, applications, and trends," ISPRS Journal of Photogrammetry and Remote Sensing, vol. 64, no. 4, pp. 335-344, 2009/07/01/ 2009, doi: https://doi.org/10.1016/j.isprsjprs.2009.03.007.

[24] Z. Qin, A. Karnieli, and P. Berliner, "A mono-window algorithm for retrieving land surface temperature from Landsat TM data and its application to the Israel-Egypt border region," International Journal of Remote Sensing, vol. 22, no. 18, pp. 3719-3746, 2001/01/01 2001, doi: 10.1080/01431160010006971.

[25] O. Rozenstein, Z. Qin, Y. Derimian, and A. Karnieli, "Derivation of Land Surface Temperature for Landsat-8 TIRS Using a Split Window Algorithm," Sensors, vol. 14, no. 4, pp. 5768-5780, 2014. [Online]. Available: https://www.mdpi.com/1424-8220/14/4/5768.

[26] L. Liang et al., "Estimation of crop LAI using hyperspectral vegetation indices and a hybrid inversion method," Remote Sensing of Environment, vol. 165, pp. 123-134, 2015/08/01/ 2015, doi: https://doi.org/10.1016/j.rse.2015.04.032.